

## Cluster-counterpart Voids: Void Identification from Galaxy Density Field

JUNSUP SHIM <sup>1,2</sup> CHANGBOM PARK,<sup>1</sup> JUHAN KIM <sup>3</sup>, AND SUNGWOOK E. HONG(홍성욱) <sup>4,5</sup>

<sup>1</sup>*School of Physics, Korea Institute for Advanced Study, 85 Hoegiro, Dongdaemun-gu, Seoul 02455, Korea*

<sup>2</sup>*Institute of Astronomy and Astrophysics, Academia Sinica, No.1, Sec. 4, Roosevelt Rd, Taipei 10617, Taiwan*

<sup>3</sup>*Center for Advanced Computation, Korea Institute for Advanced Study, 85 Hoegiro, Dongdaemun-gu, Seoul 02455, Korea*

<sup>4</sup>*Korea Astronomy and Space Science Institute, 776 Daedeokdae-ro, Yuseong-gu, Daejeon 34055, Korea*

<sup>5</sup>*Astronomy Campus, University of Science & Technology, 776 Daedeok-daero, Yuseong-gu, Daejeon 34055, Korea*

### ABSTRACT

We identify cosmic voids from galaxy density fields under the theory of void-cluster correspondence. We extend the previous novel void-identification method developed for the matter density field to the galaxy density field for practical applications. From cosmological N-body simulations, we construct galaxy number- and mass-weighted density fields to identify cosmic voids that are counterparts of galaxy clusters of specific mass. The parameters for the cluster-counterpart void identification such as Gaussian smoothing scale, density threshold, and core volume fraction are found for galaxy density fields. We achieve about 60–67% of completeness and reliability for identifying the voids of corresponding cluster mass above  $3 \times 10^{14} h^{-1} M_{\odot}$  from a galaxy sample with the mean number density,  $\bar{n} = 4.4 \times 10^{-3} (h^{-1} \text{Mpc})^{-3}$ . When the mean density is increased to  $\bar{n} = 10^{-2} (h^{-1} \text{Mpc})^{-3}$ , the detection rate is enhanced by  $\sim 2$ –7% depending on the ‘mass scale’ of voids. We find that the detectability is insensitive to the density weighting scheme applied to generate the density field. Our result demonstrates that we can apply this method to the galaxy redshift survey data to identify cosmic voids corresponding statistically to the galaxy clusters in a given mass range.

*Keywords:* Large-scale structure of the universe (902), Voids (1779)

### 1. INTRODUCTION

Cosmic voids are the largest volume component of the large-scale structures in the universe (Joeveer & Einasto 1978; Einasto et al. 1980; Gott et al. 1986; de Lapparent et al. 1986; Vogeley et al. 1994) but contain a relatively small amount of mass. Because of their underdense nature, voids have been utilized as a probe for dark energy (Lee & Park 2009; Lavaux & Wandelt 2010; Li 2011; Pisani et al. 2015; Sutter et al. 2015; Achitouv 2017), gravitation (Nusser et al. 2005; Li et al. 2012; Cai et al. 2015; Achitouv 2019), initial conditions (Kim & Park 1998), as well as a laboratory for studying the environmental effect on galaxy formation and evolution (Ceccarelli et al. 2008; Park & Lee 2009; Kreckel et al. 2011; Beygu et al. 2013; Shim et al. 2015; Ceccarelli et al. 2022).

For void identification from simulation and observation, various void-finding methods have been developed (Kauffmann & Fairall 1991; El-Ad et al. 1996; Colberg et al. 2005; Patiri et al. 2006b; Hahn et al. 2007; Platen et al. 2007; Neyrinck 2008; Forero-Romero et al. 2009; Lavaux & Wandelt 2010; Sutter et al. 2015; Shim et al. 2021). With reasonable void-finding parameter values, a void-finder may identify voids that are aspherical and hierarchical. However, neither the asphericity nor hierarchical structure of voids are taken into account in the spherical void formation model (Fillmore & Goldreich 1984; Suto et al. 1984; Bertschinger 1985). Thus, it is not unnatural to find some discrepancy between voids in data and the spherical void model. For example, the shell-crossing density threshold derived from the statistics of voids in data is inconsistent with the prediction based on the spherical void approximation (Chan et al. 2014; Achitouv et al. 2015; Nadathur & Hotchkiss 2015). This motivates a search for a new definition and identification method for voids that mitigate the inconsistency between voids in theory and data.

Recently, a new concept of defining voids has been presented (Pontzen et al. 2016; Shim et al. 2021; Stopyra et al. 2021; Desmond et al. 2022). The key idea of void identification in these studies is that a void of a certain size can be related with a dark matter halo of a particular mass because a halo region would have become a void if the initial overdensity field were inverted. The correspondence between voids and dark matter halos in the inverted field is more reliable on the scale of massive galaxy clusters. This argument leads us to define cosmic voids as counterpart to galaxy clusters, and we will call the void of a certain size identified and related with the cluster of corresponding mass, the *cluster-counterpart void* (CCV). Other interesting features of CCVs include 1) almost universal density profiles (Shim et al. 2021) and 2) their mean density contrast being close to the prediction from the spherical expansion model (Stopyra et al. 2021; Desmond et al. 2022). Interestingly, 3) they are still in the quasi-linear regime, and information on the initial conditions is better preserved relative to clusters (Kim & Park 1998; Stopyra et al. 2021).

In order to identify CCVs from a given density field, two different approaches have been suggested. The major difference between the two approaches is whether the void identification method requires the reconstruction of the initial density fields. Without utilizing the initial density field, Shim et al. (2021) established a simple CCV identification method adopting free parameters for smoothing scale, density and volume thresholds. On the other hand, reversely evolving a given density field to the initial state and then forwardly evolving its sign-inverted density fluctuation field to the present epoch to identify CCVs was suggested by Stopyra et al. (2021) and implemented by Desmond et al. (2022). In this study, we extend and apply the former approach adopted in Shim et al. (2021) to galaxy density fields.

This paper is organized as follows. We describe our simulations and the scheme for assigning galaxies to halos in Section 2. In Section 3, we briefly review the identification of CCVs from dark matter density fields and describe how we apply this approach to galaxy density fields in Section 4. We discuss our results and conclude in Section 5.

## 2. SIMULATION AND GALAXY MOCKS

We use a pair of N-body simulations with inverted initial overdensity fields to study the CCVs and their corresponding clusters. The Mirror simulation used in this work is one of the Multiverse simulations introduced by Park et al. (2019) and Tonegawa et al. (2020). The Reference simulation starts with the initial density fluctuations that have the same amplitude as in the Mir-

ror simulation but have the opposite sign. The simulations adopt the GOTPM (Dubinski et al. 2004) code and WMAP 5-year  $\Lambda$ CDM cosmology (Dunkley et al. 2009) with the matter, baryon, dark energy density parameters set to 0.26, 0.044, and 0.74, respectively. Each simulation evolves  $N_p = 2048^3$  dark matter particles with mass  $m_p \simeq 9 \times 10^9 h^{-1} M_\odot$  in a periodic cubic box of side length  $L_{\text{box}} = 1024 h^{-1} \text{Mpc}$ .

We identify dark matter halos with 30 or more particles using the Friend-of-Friend (FoF) algorithm with the linking length  $l_{\text{link}} = 0.2\bar{l}_p$ , where  $\bar{l}_p$  is the mean particle separation. We then populate the identified halos with mock galaxies based on the most bound member particle (MBP)–galaxy correspondence model (Hong et al. 2016). In this galaxy assignment scheme, all MBPs marked in halo merger trees are the proxies for galaxies (De Lucia et al. 2004; Faltenbacher & Diemand 2006). The position and velocity of a galaxy are taken from those of a MBP, whereas galaxy luminosity is determined by the abundance matching between the mass function of mock galaxies (see Hong et al. 2016, for the definition of galaxy mass) and the luminosity function of the SDSS main galaxies (Choi et al. 2007). The survival time of a satellite halo is given by the merger time scale modeled with a modified version of the fitting formula described in Jiang et al. (2008). We set the power-law index of the host-to-satellite mass ratio to 1.5. This is to yield a good match for the projected two-point correlation functions between the mock galaxies in our simulations and SDSS main galaxies down to scales below  $1 h^{-1} \text{Mpc}$  (Zehavi et al. 2011).

We construct two galaxy samples with different mean number densities to test the effect of sample density on the CCV identification. The mean number densities of the sparse and dense samples are  $\bar{n}_{\text{gal}} = 4.4 \times 10^{-3}$  and  $1.0 \times 10^{-2} h^3 \text{Mpc}^{-3}$ , respectively. We chose the sparse sample density as such assuming that the sparse galaxy sample mimics a volume-limited sample from the SDSS main galaxy sample with the largest survey volume (Choi et al. 2010). For the dense sample, its mean density is set close to the highest achievable density from the simulations. The dense sample-like data will be available from upcoming surveys such as Dark Energy Spectroscopic Instrument (DESI Collaboration et al. 2016) and SPHEREx (Doré et al. 2014) given that their expected number densities of observed galaxies up to  $z \approx 0.2$  are higher than our dense sample density.

## 3. IDENTIFYING CCVS WITH DARK MATTER

We briefly summarize how CCVs are defined using a paired simulations in Section 3.1 and are recovered in

dark matter density fields without using the inverted simulation in Section 3.2.

### 3.1. Cluster-counterpart voids

In Figure 1, we illustrate how CCVs are identified using the Reference and Mirror simulations. We note that the cluster-scale dark matter halos in the Mirror simulation become large voids in the Reference simulation. Therefore, the dark matter particles belonging to each cluster-scale halo in one simulation can be used to define the void region in the other one. Thus, each cluster in the Mirror simulation uniquely defines a CCV in the Reference simulation.

We generate a catalog containing the position, effective radius, mean and central densities of CCVs in the Reference simulation that correspond to 422,818 halos with halo mass  $M_h \geq 10^{13} h^{-1} M_\odot$  at  $z = 0$  in the Mirror simulation. The volume of a CCV is defined as the region occupied by the void member particles in the Reference simulation. A CCV associated with a more massive dark matter halo tends to have a larger volume (Shim et al. 2021).

### 3.2. CCVs from dark matter density fields

In this subsection, we describe a method developed by Shim et al. (2021) for finding the CCVs in the Reference simulation without resorting to the Mirror simulation. First, we find the most underdense regions in the smoothed density field below a certain threshold density, and then select those whose volume is larger than a certain fraction of the typical void volume. The expected typical or mean void volume is directly related with the corresponding cluster mass. Namely, a choice of cluster mass determines the corresponding CCV size, which is used to select the void core regions. Our method is based on the finding that a larger CCV tends to develop a larger *void core*, the central region with density below the specific threshold value.

There are three parameters used in this method: Gaussian smoothing scale ( $R_s$ ), core density threshold ( $\delta_c$ ), and core volume fraction ( $f_c$ ) with respect to the CCV volume at that mass scale. The optimal values of these parameters change depending on the mean void size or corresponding cluster mass. The matter density field is smoothed with a Gaussian filter over  $R_s$ , and the void core regions with overdensity below  $\delta_c$  are found. Among them those with volume larger than  $f_c$  times the typical volume of the CCVs under interest are selected. Because void cores only cover the innermost volume of CCVs, we then grow the cores by repeatedly attaching neighboring higher density volume elements. This growing process stops when the total volume of the recovered

voids reaches that of the CCVs of the interested mass scale in the Reference simulation.

## 4. IDENTIFYING CCVS FROM GALAXY DENSITY FIELDS

We test whether or not the CCV identification method originally developed for dark matter density fields could be also applied to galaxy density fields. The success of the extension of the prescription depends on how accurately the galaxy density field follows the underlying dark matter density field, especially in underdense regions. To be more specific, the rank order of pixel density should be preserved; a region with a higher dark matter density should have a higher galaxy density value if we aim to identify the same voids in the galaxy and dark matter density fields using this method. Any reversal in the rank order will disturb the correspondence. Thus, we first examine the relation between galaxy and dark matter density fields in Section 4.1 and determine the optimal values of free parameters for galaxy density fields in Section 4.2.

### 4.1. Dark matter versus Galaxy density fields

Before we develop a void finding algorithm for a galaxy sample, we first compare between number- and mass-weighted galaxy density fields to study which one has tighter relation with the underlying matter distribution. The weighted density is calculated at the center of each pixel with a volume  $(2 h^{-1} \text{Mpc})^3$  using the cloud-in-cell (CIC) assignment scheme. We then smooth these density fields with Gaussian smoothing kernel. In Figure 2, we compare between smoothed dark matter and galaxy density fields. As can be seen, the overdensities of both galaxy density fields are enhanced compared to that of the dark matter density field, which reflects galaxies being the biased tracers of the underlying matter field (Kaiser 1984; Bardeen et al. 1986; Desjacques et al. 2018). Interestingly, the non-linear relation between dark matter and galaxy density fields is well modeled by the second-order polynomials of logarithmic densities as discovered in Jee et al. (2012). Note that this relation reduces to a linear bias model when  $|\delta| \ll 1$ .

We find that the mass-weighted galaxy density is more tightly correlated with the dark matter density than the number-weighted case. The standard deviation of the logarithmic dark matter overdensity for a given logarithmic galaxy overdensity bin is on average 10% smaller in the mass-weighted galaxy field than in the number-weighted one. This is consistent with the previous results showing that mass weighting reduces the scatter between dark matter and halo density field (Park et al. 2007; Seljak et al. 2009; Park et al. 2010). However, the

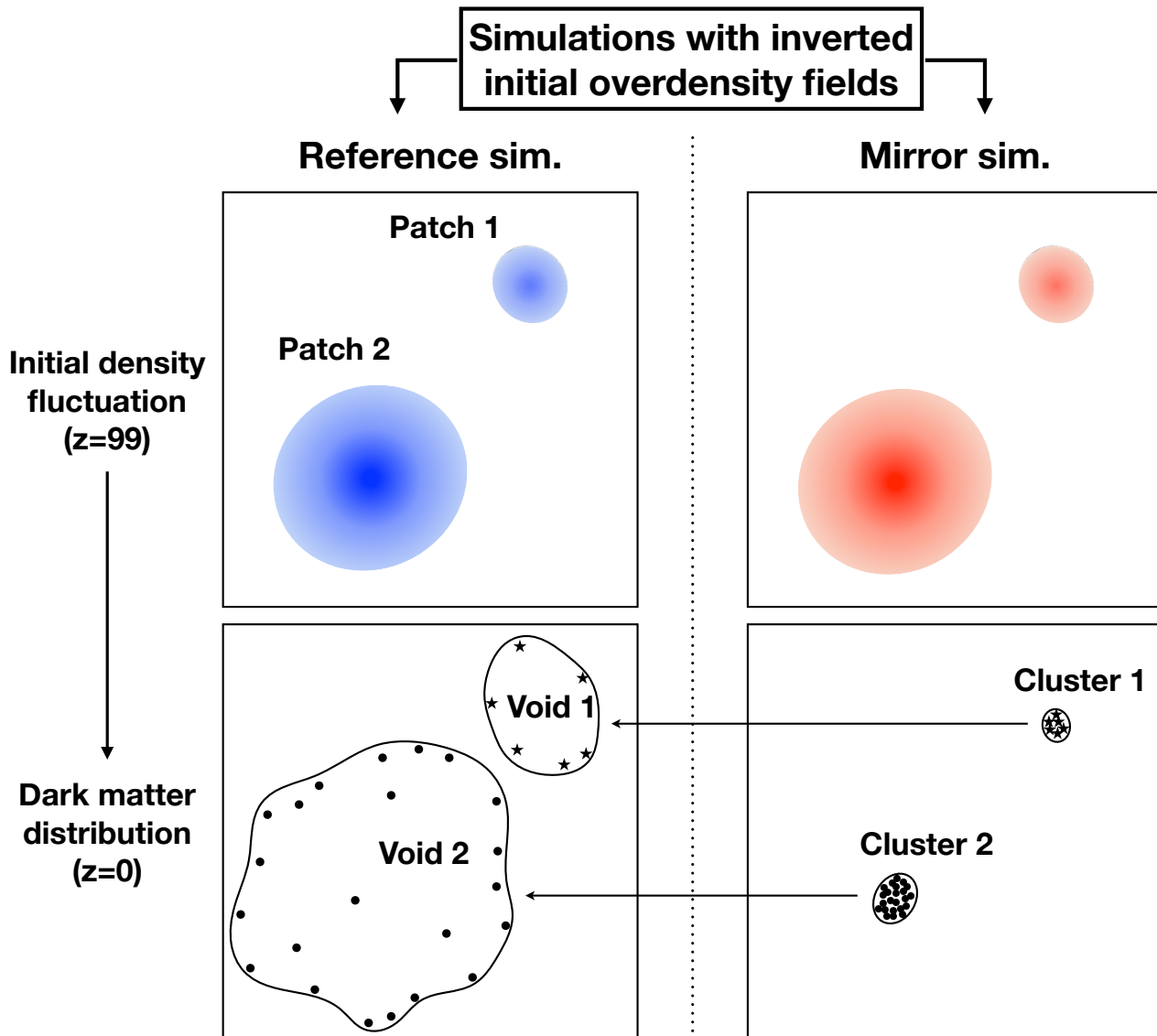


**Figure 1.** A schematic diagram showing how CCVs are identified under the paradigm of the void-cluster correspondence theory using the Reference and Mirror simulations. *Top panels:* Initial density fluctuations of the same regions within the Reference (left) and Mirror (right) simulations. The initial density troughs (blue regions) in the Reference simulation correspond to the initial density peaks (red regions) in the Mirror simulation because the initial overdensity fields of the two simulations are designed to be the sign-inverted version of the other. *Bottom panels:* Distributions of dark matter particles forming voids (left) and their counterpart clusters (right) through gravitational evolution from their initial particle distributions representing initial underdensities (top left) and overdensities (top right), respectively. Note that we illustrate only the density troughs and voids for the Reference simulation, and their corresponding density peaks and clusters for the Mirror simulation, for simplicity.

standard deviation for the mass-weighted galaxy density field becomes comparable to that for the number-weighted case at an extremely low-density range. For this reason, we consider both the number- and mass-weighted galaxy density fields even though the scatter is overall smaller in the mass-weighted case. The scatter in the relation between the galaxy and dark matter fields reflects the stochastic nature of bias (Pen 1998; Dekel & Lahav 1999; Matsubara 1999) and the shot noise effect on density measurement. Because of these two ef-

fects, the rank order of pixel values in the density array changes when we move from the matter density field to galaxy density field.

In Figure 3, we show how much the degree of randomization in the rank order depends on the density weighting scheme and smoothing scale. We compute the volume overlap fraction ( $f_{\text{overlap}}$ ) of the lowest-density regions between galaxy and dark matter density fields

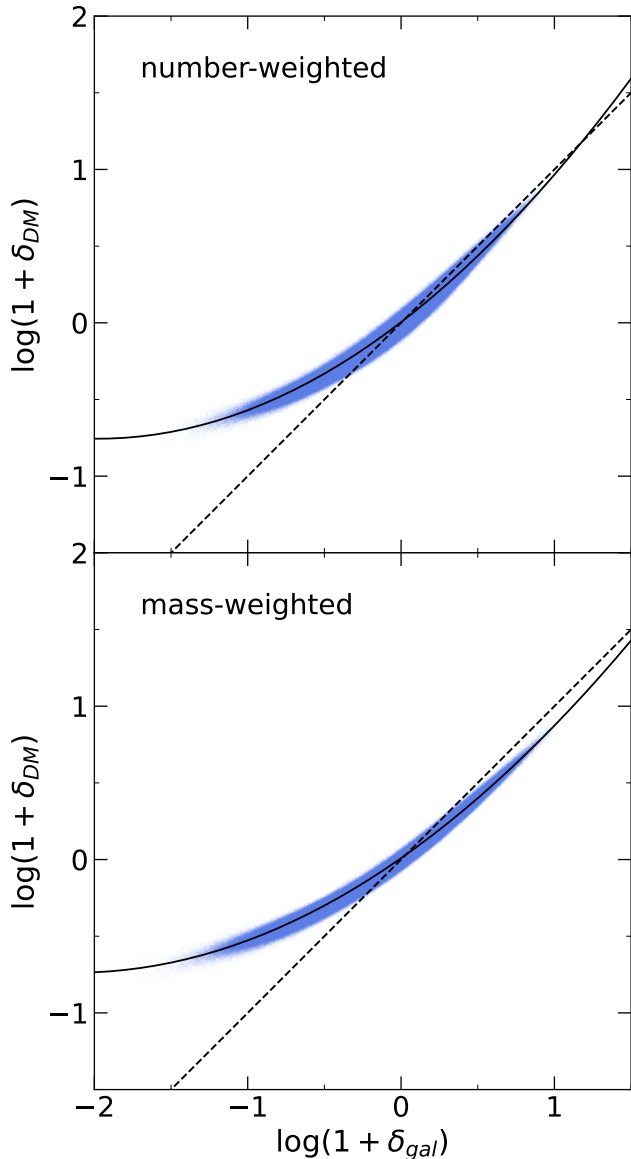


**Figure 2.** Relation between dark matter and galaxy overdensities. The upper (lower) panel shows the case for the number- (mass-)weighted galaxy density field. The Gaussian smoothing scale applied is  $R_s = 7.3 h^{-1}\text{Mpc}$ . Solid lines are the second-order polynomial fits to the relations (Jee et al. 2012), whereas dash lines represent the identity relation,  $\delta_{\text{DM}} = \delta_{\text{gal}}$ .

as

$$f_{\text{overlap}} = \frac{V_{\text{overlap}}}{V_{\text{low}}}, \quad (1)$$

where  $V_{\text{low}}$  is the volume with density lower than the input threshold and  $V_{\text{overlap}}$  is the overlap volume between those lowest-density regions in the two density fields. And the fraction of volume occupied by the

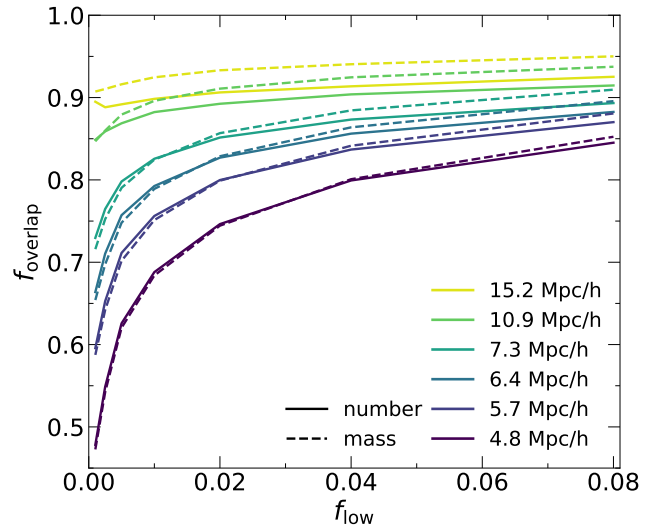


**Figure 3.** Volume overlap fraction ( $f_{\text{overlap}}$ ) of underdense regions between dark matter and galaxy density fields as a function of the volume fraction ( $f_{\text{low}}$ ) of the low-density regions. The galaxy density fields are constructed using the dense galaxy sample. Solid (dashed) lines represent number (mass)-weighted galaxy density fields. Different colors indicate various Gaussian smoothing scales.

lowest-density regions is given as

$$f_{\text{low}} = \frac{V_{\text{low}}}{V_{\text{sim}}}, \quad (2)$$

where  $V_{\text{sim}}$  is the entire simulation volume. For example,  $f_{\text{overlap}} = 0$  at  $f_{\text{low}} = 0.02$  means that the most underdense 2% volumes in galaxy and dark matter density field have no overlap between them.

We find the decreasing trend of the volume overlap fraction toward a lower  $f_{\text{low}}$ , which becomes steeper for a smaller smoothing scale. This implies that the order shuffling between two density fields is severe at the center of voids, or in the most underdense regions. It is also shown that the overlap fraction is higher for a larger smoothing scale implying that the shuffling becomes less significant when galaxy density fields are smoothed on relatively larger smoothing scales. However, the density order at extreme low-density range is still changed by  $\sim 10$  per cent for the largest smoothing scale.

#### 4.2. Optimal parameter values for CCV Identification

We need to fine-tune the free parameters for CCV identification in the galaxy density field. This is because galaxy density field is non-linearly biased with respect to the underlying dark matter density field, and hence the fine-tuned parameters obtained for the dark matter field can not be applied to the galaxy density field without adjustment. We thus follow the approach described in Shim et al. (2021). The optimal values of the free

parameters are determined so that completeness and reliability are maximized. We calculate the completeness and reliability of void finding given by

$$\mathcal{C} \equiv N_s/N_v, \quad (3)$$

and

$$\mathcal{R} \equiv N_s/N_c, \quad (4)$$

respectively. Here,  $N_v$ ,  $N_c$ , and  $N_s$  represent the number of the CCVs of a target mass scale, all the identified void cores, and successfully-reproduced CCVs, respectively. From here on, the mass scale of a CCV refers to the corresponding cluster mass.

The completeness represents the successfully recovered fraction among the CCVs with the corresponding cluster mass above  $M_{\min}$ . On the other hand, the reliability is the fraction of recovered voids with the corresponding  $M \geq 0.8M_{\min}$  (to allow for a buffer in mass) among all the identified voids by this method. Here, it is counted as a successful detection when the nearest CCV from the identified void core satisfies the mass criterion or when the most massive CCV within  $1.5r_c$  from the void core satisfies the mass criterion. Here,  $r_c$  is the effective radius of the void core and is measured from the void core volume  $V_c$  using the following relation

$$r_c = \left( \frac{3V_c}{4\pi} \right)^{\frac{1}{3}}. \quad (5)$$

We repeat calculating the detection completeness and reliability in three dimensional parameter space of  $R_s$ ,  $\delta_c$ , and  $f_c$ , and provide their optimal values in Table 1. Note that we limit the smoothing scales to be the reciprocals of integers multiplied by the effective radius of the CCVs of the target mass scale. The optimal length scales for smoothing galaxy density fields are  $R_s = R_v/3$  in most cases, where  $R_v$  is the effective radius of a CCV of a particular mass scale. This implies that the optimized smoothing scale of a given galaxy density field is determined by the target mass scale, or equivalently the target size, of voids. Interestingly, the relation between the smoothing scale and void size is consistent with the case for the dark matter density fields (Shim et al. 2021).

In Figure 4, we show the detection completeness and reliability for different minimum target mass scales of CCVs. It is shown that the detection completeness, and equivalently the reliability, does not depend much on the density-weighting scheme. On the other hand, the mean galaxy number density significantly affects the detection quality. This is just because of the unavoidable nature of the cosmic voids whose identification is sensitive to the tracer number density. For the sparse sample, the detection rates increase from  $\mathcal{C} = \mathcal{R} = 0.60$  to 0.66 with

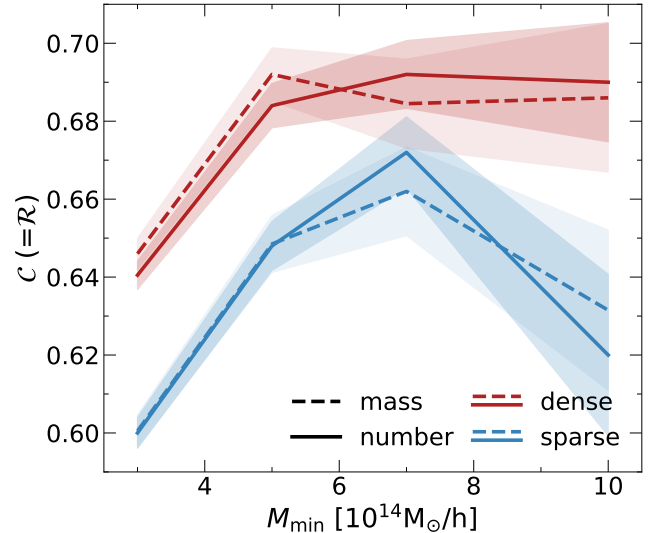


**Figure 4.** Completeness and reliability of identifying CCVs from the mass-weighted (dashed) and number-weighted (solid) density fields constructed using the dense (red) and sparse (blue) galaxy sample. The shaded regions are the detection rate uncertainties calculated as the standard deviations of the completeness and reliability measured from bootstrap resampled galaxy density fields. The detection rates and uncertainties are calculated when the optimal parameter values in Table 1 are adopted. Note that the completeness and reliability are identical for the optimal parameter values.

the void mass scale before  $M_{\min} \simeq 7 \times 10^{14} h^{-1}M_{\odot}$ , and then they drop to 0.62 at  $M_{\min} = 10^{15} h^{-1}M_{\odot}$ . When using the dense sample, the detection rates are enhanced approximately by 2 – 7%. This is because the dense sample includes low mass galaxies that are more likely to be in voids than in other environments (Alonso et al. 2015). Thus, increasing sample density decreases the shot noise effect, and hence the density-order shuffling in underdense regions. The detection rate enhancement is most noticeable at the largest mass scale,  $M_{\min} = 10^{15} h^{-1}M_{\odot}$ . Because the halo abundance in a large void is lower than in a small void (Patiri et al. 2006a), increasing the sample density by adding lower-mass galaxies has more significant effect on decreasing the shot-noise for larger voids. Consequently, the density-order shuffling diminishes, leading to the rapid increase in the detection rate at the largest mass scale. In line with this interpretation, we find that the uncertainty of the detection rate, which increases with the void mass scale, are the largest for the largest scale voids. We compute the uncertainty as the standard deviation of the detection rate measured from 1000 realizations of bootstrap resampled galaxy density fields. More importantly, increasing sample density reduces the uncertainties of the detection rates approximately by 26% and

**Table 1.** Optimal values of the free parameters for the CCV identification from galaxy density fields constructed using the dense and sparse galaxy samples. The upper (lower) half of the table corresponds to the number- (mass-)weighted galaxy density fields. Listed in columns are the mean galaxy number density  $\bar{n}_{\text{gal}}$ , minimum target mass scale of a CCV  $M_{\text{min}}$ , effective radius of the CCV  $R_v$ , smoothing scale  $R_s$ , core density threshold  $\delta_c$ , upper density threshold  $\delta_{\text{upper}}$  when core growing stops, and minimum core fraction  $f_c$ .

	$\bar{n}_{\text{gal}}$ [(Mpc/h) <sup>-3</sup> ]	$M_{\text{min}}$ [10 <sup>14</sup> M <sub>⊙</sub> /h]	$R_v$ [Mpc/h]	$R_s$ [R <sub>v</sub> ]	$\delta_c$	$\delta_{\text{upper}}$	$f_c$
number-weighted	$1.0 \times 10^{-2}$	3	14.5	1/4	-0.981	-0.785	0.02
		5	17.2	1/3	-0.915	-0.738	0.02
		7	19.3	1/3	-0.923	-0.725	0.01
		10	21.7	1/3	-0.890	-0.727	0.05
	$4.4 \times 10^{-3}$	3	14.5	1/4	-0.995	-0.853	0.01
		5	17.2	1/4	-0.981	-0.858	0.05
		7	19.3	1/4	-0.967	-0.861	0.10
		10	21.7	1/2	-0.835	-0.619	0.01
mass-weighted	$1.0 \times 10^{-2}$	3	14.5	1/4	-0.987	-0.835	0.02
		5	17.2	1/3	-0.928	-0.797	0.03
		7	19.3	1/3	-0.942	-0.779	0.01
		10	21.7	1/3	-0.921	-0.771	0.04
	$4.4 \times 10^{-3}$	3	14.5	1/4	-0.996	-0.894	0.01
		5	17.2	1/3	-0.957	-0.829	0.02
		7	19.3	1/3	-0.950	-0.824	0.03
		10	21.7	1/3	-0.937	-0.816	0.05

7% at the largest void mass scale, whereas they only decreased by 7.6% and 3.7% on average on smaller mass scales for the number- and mass-weighted cases, respectively. Thus, the benefit of increasing galaxy sample density is most significant in the largest CCV detection.

Finally, we show in Figure 5 the spatial correspondence between the recovered voids (black contours) using this method and the CCVs (colored regions) defined under the void-cluster correspondence theory. The voids are recovered from the number-weighted galaxy density fields constructed using the dense galaxy sample. It is shown that the recovered void regions well overlap with the CCVs of the target mass scales. A recovered void typically corresponds to a single CCV unless the corresponding CCV has neighboring CCVs. This nearly one-to-one correspondence between a recovered void and a CCV becomes relatively weaker for a smaller minimum target void mass. Thus, the trend of a recovered void encompassing multiple CCVs is most noticeable for  $M_{\text{void}} > 3 \times 10^{14} h^{-1} M_{\odot}$ . However, in principle, by comparing recovered void regions for two different target mass scales one can decompose such void complexes into several smaller voids that respectively correspond to single CCVs.

## 5. SUMMARY AND DISCUSSION

We identify cosmic voids from galaxy density fields under the void-cluster correspondence theory. The cor-

respondence between voids and clusters of the same mass scale is established using paired cosmological simulations with sign-opposite initial overdensity fields. Cluster-counterpart voids (CCVs) in one simulation are defined as the regions occupied by the same dark matter particles that form cluster-scale halos in its inverted simulation.

Extending the CCV-identification method (Shim et al. 2021) developed for matter density fields, we find the optimal values of the free parameters for the void identification in galaxy density fields; Gaussian smoothing scale, density threshold, and core volume fraction. The optimal length scale for smoothing galaxy density fields is determined by the target mass scale of voids, which is related to the target void radius as  $R_s = R_v/3$ . The optimal parameter values for the number- and mass-weighted density fields constructed using the sparse and dense galaxy samples are listed in Table 1. Using the dense galaxy sample, we can achieve about 64 – 69% of CCV detection completeness and reliability from the number-weighted galaxy density fields. The detection rates decrease by  $\sim 2 - 7\%$  when using the sparse galaxy sample due to increasing effects of shot-noise on density.

Our result demonstrates that we can identify CCVs from galaxy density fields in real space. In actual galaxy surveys, on the other hand, one needs to consider the redshift-space distortion (RSD) when constructing den-

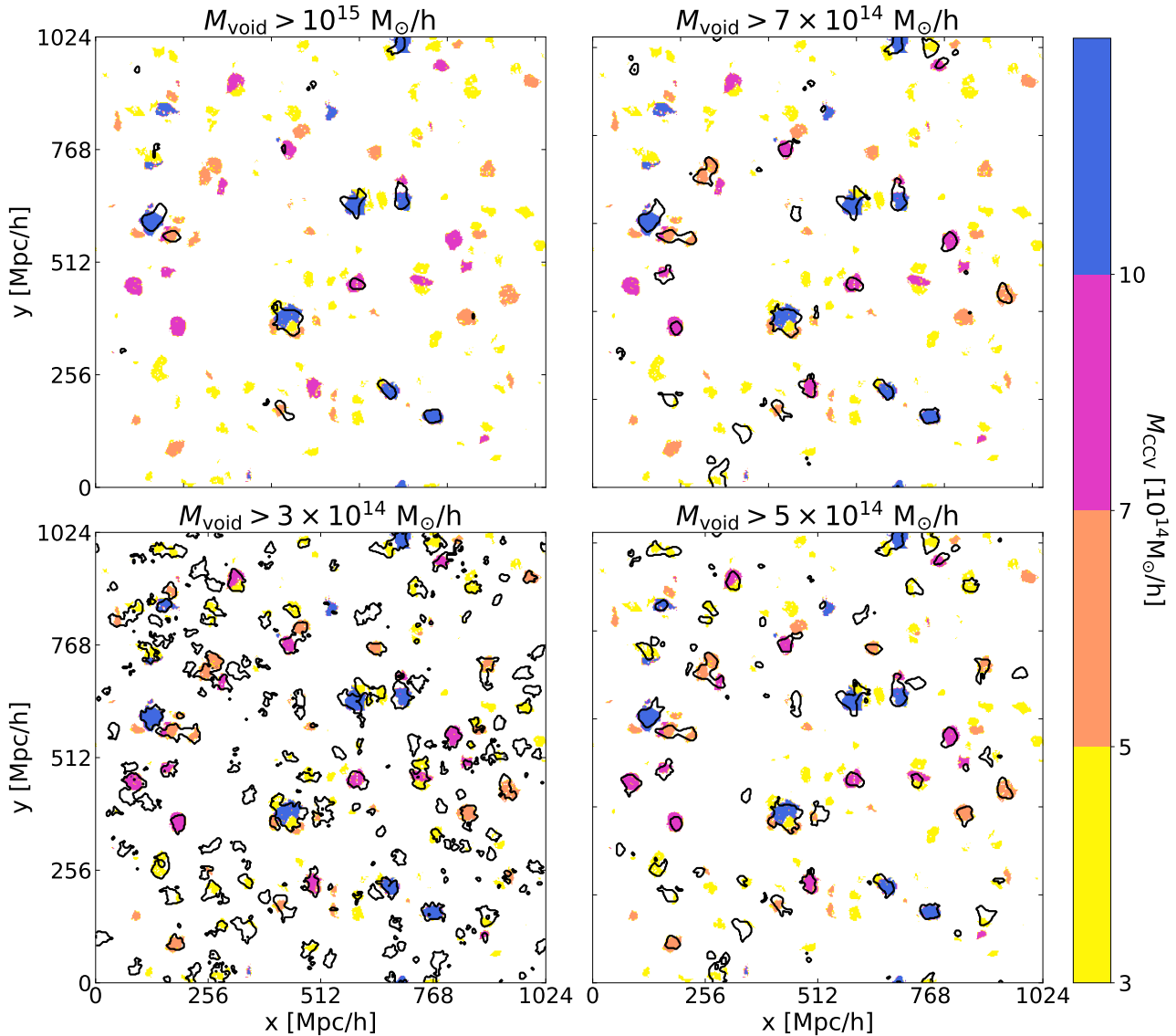


**Figure 5.** Recovered voids (black contours) from the number-weighted galaxy density fields and CCVs (non-black) of various mass scales in a  $2 h^{-1}\text{Mpc}$ -thick slice. The optimal parameter values listed in Table 1 are adopted. All panels show the identical field. Recovered voids corresponding to galaxy cluster mass scale above  $1 \times 10^{15}$ ,  $7 \times 10^{14}$ ,  $5 \times 10^{14}$  and  $3 \times 10^{14} h^{-1}M_{\odot}$  are shown in clockwise direction from the upper-left panel to bottom-left.

sity fields from the observed galaxy distribution in redshift space. Directly identifying CCVs in redshift space without considering the RSD effect will be less reliable than in real space. This is because the RSD further introduces the density-rank order randomization in addition to those induced by the shot-noise and stochasticity of bias. Thus, it is better to adopt reconstruction techniques and identify CCVs in real space than in redshift space. The fingers of God (Jackson 1972) due to the internal motion of galaxies within clusters can be effectively removed by forcing the line-of-sight elongation of clusters equal to their size perpendicular to the line-of-sight (Tegmark et al. 2004; Park et al. 2012;

Tully 2015; Hwang et al. 2016). On larger scales, the Kaiser effect (Kaiser 1987) due to coherent flow induced by large-scale over/under-densities can be corrected using Zel’dovich approximation (Zel’Dovich 1970) or second order Lagrangian perturbation theory (Scoccimarro 1998). Using these approaches, one can place galaxies back to their real space positions by subtracting the displacement due to their peculiar motions (Wang et al. 2009; Kitaura et al. 2012; Bos et al. 2019).

Identifying CCVs from observational data could help us perform more precise cosmological and astrophysical analysis using voids. Because CCVs have universal mass density distribution (Shim et al. 2021) and com-



mon central and average densities (Pontzen et al. 2016; Stopyra et al. 2021; Desmond et al. 2022), they represent relatively more homogeneous void population than arbitrary underdense regions extracted from density fields. Consequently, when using CCVs it is possible to decrease the uncertainties arising due to the scatter in void properties. This will be the subject of a future study. One of the possible applications of CCVs in the cosmological context is to measure the linear growth rate using CCVs. In addition to the homogenous properties of the CCVs, their internal dynamics remain near linear (Stopyra et al. 2021), and the linear bias relation holds at around CCVs (Pollina et al. 2017). Because the linearity in and around the CCV environment allows a simple linear modeling for void-galaxy cross-correlation accurate measurements of linear growth rate using voids (Achitouv 2019; Hamaus et al. 2022; Woodfinden et al. 2022) can be made using CCVs. We leave such cos-

mological analysis using CCVs from galaxy surveys to future work.

#### ACKNOWLEDGEMENTS

We thank an anonymous referee for helpful comments that helped improve the original manuscript. J.S. and C.B.P. were supported by KIAS Individual Grant PG071202 and PG016903 at Korea Institute for Advanced Study, respectively. J.K. was supported by a KIAS Individual Grant (KG039603) via the Center for Advanced Computation at Korea Institute for Advanced Study. S.E.H. was supported by the project 우주거대구조를 이용한 암흑우주연구 (“Understanding the Dark Universe Using Large Scale Structure of the Universe”), funded by the Ministry of Science. The computing resources were kindly provided by the Center for Advanced Computation at Korea Institute for Advanced Study.

#### REFERENCES

- Achitouv, I. 2017, *PhRvD*, 96, 083506  
—, 2019, *PhRvD*, 100, 123513  
Achitouv, I., Neyrinck, M., & Paranjape, A. 2015, *MNRAS*, 451, 3964  
Alonso, D., Eardley, E., & Peacock, J. A. 2015, *MNRAS*, 447, 2683  
Bardeen, J. M., Bond, J. R., Kaiser, N., & Szalay, A. S. 1986, *ApJ*, 304, 15  
Bertschinger, E. 1985, *ApJS*, 58, 1  
Beygu, B., Kreckel, K., van de Weygaert, R., van der Hulst, J. M., & van Gorkom, J. H. 2013, *AJ*, 145, 120  
Bos, E. G. P., Kitaura, F.-S., & van de Weygaert, R. 2019, *MNRAS*, 488, 2573  
Cai, Y.-C., Padilla, N., & Li, B. 2015, *MNRAS*, 451, 1036  
Ceccarelli, L., Duplancic, F., & Garcia Lambas, D. 2022, *MNRAS*, 509, 1805  
Ceccarelli, L., Padilla, N., & Lambas, D. G. 2008, *MNRAS*, 390, L9  
Chan, K. C., Hamaus, N., & Desjacques, V. 2014, *PhRvD*, 90, 103521  
Choi, Y.-Y., Park, C., Kim, J., et al. 2010, *ApJS*, 190, 181  
Choi, Y.-Y., Park, C., & Vogeley, M. S. 2007, *ApJ*, 658, 884  
Colberg, J. M., Sheth, R. K., Diaferio, A., Gao, L., & Yoshida, N. 2005, *MNRAS*, 360, 216  
de Lapparent, V., Geller, M. J., & Huchra, J. P. 1986, *ApJL*, 302, L1  
De Lucia, G., Kauffmann, G., & White, S. D. M. 2004, *MNRAS*, 349, 1101  
Dekel, A., & Lahav, O. 1999, *ApJ*, 520, 24  
DESI Collaboration, Aghamousa, A., Aguilar, J., et al. 2016, arXiv e-prints, arXiv:1611.00036  
Desjacques, V., Jeong, D., & Schmidt, F. 2018, *PhR*, 733, 1  
Desmond, H., Hutt, M. L., Devriendt, J., & Slyz, A. 2022, *MNRAS*, 511, L45  
Doré, O., Bock, J., Ashby, M., et al. 2014, arXiv e-prints, arXiv:1412.4872  
Dubinski, J., Kim, J., Park, C., & Humble, R. 2004, *NewA*, 9, 111  
Dunkley, J., Komatsu, E., Nolta, M. R., et al. 2009, *ApJS*, 180, 306  
Einasto, J., Jooevar, M., & Saar, E. 1980, *MNRAS*, 193, 353  
El-Ad, H., Piran, T., & da Costa, L. N. 1996, *ApJL*, 462, L13  
Faltenbacher, A., & Diemand, J. 2006, *MNRAS*, 369, 1698  
Fillmore, J. A., & Goldreich, P. 1984, *ApJ*, 281, 9  
Forero-Romero, J. E., Hoffman, Y., Gottlöber, S., Klypin, A., & Yepes, G. 2009, *MNRAS*, 396, 1815  
Gott, J. Richard, I., Melott, A. L., & Dickinson, M. 1986, *ApJ*, 306, 341  
Hahn, O., Porciani, C., Carollo, C. M., & Dekel, A. 2007, *MNRAS*, 375, 489  
Hamaus, N., Aubert, M., Pisani, A., et al. 2022, *A&A*, 658, A20  
Hong, S. E., Park, C., & Kim, J. 2016, *ApJ*, 823, 103  
Hwang, H. S., Geller, M. J., Park, C., et al. 2016, *ApJ*, 818, 173  
Jackson, J. C. 1972, *MNRAS*, 156, 1P  
Jee, I., Park, C., Kim, J., Choi, Y.-Y., & Kim, S. S. 2012, *ApJ*, 753, 11

- Jiang, C. Y., Jing, Y. P., Faltenbacher, A., Lin, W. P., & Li, C. 2008, *ApJ*, 675, 1095
- Joeveer, M., & Einasto, J. 1978, in *Large Scale Structures in the Universe*, ed. M. S. Longair & J. Einasto, Vol. 79, 241
- Kaiser, N. 1984, *ApJL*, 284, L9
- . 1987, *MNRAS*, 227, 1
- Kauffmann, G., & Fairall, A. P. 1991, *MNRAS*, 248, 313
- Kim, M., & Park, C. 1998, *Journal of Korean Astronomical Society*, 31, 109
- Kitaura, F.-S., Angulo, R. E., Hoffman, Y., & Gottlöber, S. 2012, *MNRAS*, 425, 2422
- Kreckel, K., Platen, E., Aragón-Calvo, M. A., et al. 2011, *AJ*, 141, 4
- Lavaux, G., & Wandelt, B. D. 2010, *MNRAS*, 403, 1392
- Lee, J., & Park, D. 2009, *ApJL*, 696, L10
- Li, B. 2011, *MNRAS*, 411, 2615
- Li, B., Zhao, G.-B., & Koyama, K. 2012, *MNRAS*, 421, 3481
- Matsubara, T. 1999, *ApJ*, 525, 543
- Nadathur, S., & Hotchkiss, S. 2015, *MNRAS*, 454, 2228
- Neyrinck, M. C. 2008, *MNRAS*, 386, 2101
- Nusser, A., Gubser, S. S., & Peebles, P. J. 2005, *PhRvD*, 71, 083505
- Park, C., Choi, Y.-Y., Kim, J., et al. 2012, *ApJL*, 759, L7
- Park, C., Choi, Y.-Y., Vogeley, M. S., et al. 2007, *ApJ*, 658, 898
- Park, D., & Lee, J. 2009, *MNRAS*, 400, 1105
- Park, H., Kim, J., & Park, C. 2010, *ApJ*, 714, 207
- Park, H., Park, C., Sabiu, C. G., et al. 2019, *ApJ*, 881, 146
- Patiri, S. G., Betancort-Rijo, J., & Prada, F. 2006a, *MNRAS*, 368, 1132
- Patiri, S. G., Betancort-Rijo, J. E., Prada, F., Klypin, A., & Gottlöber, S. 2006b, *MNRAS*, 369, 335
- Pen, U.-L. 1998, *ApJ*, 504, 601
- Pisani, A., Sutter, P. M., Hamaus, N., et al. 2015, *PhRvD*, 92, 083531
- Platen, E., van de Weygaert, R., & Jones, B. J. T. 2007, *MNRAS*, 380, 551
- Pollina, G., Hamaus, N., Dolag, K., et al. 2017, *MNRAS*, 469, 787
- Pontzen, A., Slosar, A., Roth, N., & Peiris, H. V. 2016, *PhRvD*, 93, 103519
- Scoccimarro, R. 1998, *MNRAS*, 299, 1097
- Seljak, U., Hamaus, N., & Desjacques, V. 2009, *PhRvL*, 103, 091303
- Shim, J., Lee, J., & Hoyle, F. 2015, *ApJ*, 815, 107
- Shim, J., Park, C., Kim, J., & Hwang, H. S. 2021, *ApJ*, 908, 211
- Stopyra, S., Peiris, H. V., & Pontzen, A. 2021, *MNRAS*, 500, 4173
- Suto, Y., Sato, K., & Sato, H. 1984, *Progress of Theoretical Physics*, 71, 938
- Sutter, P. M., Lavaux, G., Hamaus, N., et al. 2015, *Astronomy and Computing*, 9, 1
- Tegmark, M., Blanton, M. R., Strauss, M. A., et al. 2004, *ApJ*, 606, 702
- Tonegawa, M., Park, C., Zheng, Y., et al. 2020, *ApJ*, 897, 17
- Tully, R. B. 2015, *AJ*, 149, 171
- Vogeley, M. S., Park, C., Geller, M. J., Huchra, J. P., & Gott, J. Richard, I. 1994, *ApJ*, 420, 525
- Wang, H., Mo, H. J., Jing, Y. P., et al. 2009, *MNRAS*, 394, 398
- Woodfinden, A., Nadathur, S., Percival, W. J., et al. 2022, *MNRAS*, arXiv:2205.06258
- Zehavi, I., Zheng, Z., Weinberg, D. H., et al. 2011, *ApJ*, 736, 59
- Zel'Dovich, Y. B. 1970, *A&A*, 500, 13